Journal of Power Sources 195 (2010) 8089–8093

Contents lists available at ScienceDirect

Journal of Power Sources

journal homepage: www.elsevier.com/locate/jpowsour

Short communication

Durability of PEM fuel cell cathode in the presence of Fe^{3+} and Al^{3+}

Hui Li[a], Ken Tsay[a], Haijiang Wang[a], Jun Shen[a], Shaohong Wu[a], Jiujun Zhang[a,*], Nengyou Jia[b], Silvia Wessel[b], Rami Abouatallah[c], Nathan Joos[c], Jeremy Schrooten[d]

[a] Institute for Fuel Cell Innovation, National Research Council of Canada, 4250 Wesbrook Mall, Vancouver, B.C. V6T 1W5, Canada
[b] Ballard Power Systems Inc., Burnaby, B.C. V5J 5J8, Canada
[c] Hydrogenics Corp., Mississauga, O.N. L5R 1B8, Canada
[d] Angstrom Power Inc., North Vancouver, B.C. V7P 3N4, Canada

ARTICLE INFO

Article history:
Received 26 May 2010
Received in revised form 30 June 2010
Accepted 1 July 2010
Available online 8 July 2010

Keywords:
PEM fuel cells
Air impurity
Metal ion contamination
Electrode kinetics
Membrane resistance

ABSTRACT

The contamination effects of Fe^{3+} and Al^{3+} on the performance of polymer electrolyte membrane fuel cells were investigated by continuously injecting Fe^{3+} or Al^{3+} salt solution into the air stream of an operating fuel cell. Both metal ions individually caused significant cell performance degradation at a level of only 5 ppm mol in air. In addition, elevated temperature accelerated fuel cell performance degradation in the presence of Fe^{3+}. Moreover, the presence of Fe^{3+} in an operating fuel cell resulted in the cell's sudden death, due to the formation of membrane pinholes that may have been promoted by the enhanced production of peroxy radicals catalyzed by Fe species. Half-cell tests in liquid electrolyte revealed that the presence of Al^{3+} in the electrolyte changed the kinetics and mechanisms of the oxygen reduction reaction by reducing the kinetic current densities and the electron transfer number.

1. Introduction

Insufficient durability and reliability caused by performance degradation are one of the greatest technical barriers for the commercialization of proton exchange membrane (PEM) fuel cells. Performance degradation can result from several causes, including Pt agglomeration [1,2], carbon corrosion [3,4], membrane degradation [5,6] and contamination [7–9], among which contamination is caused by the adverse effects of impurities on cell performance. As several studies have identified in recent years, impurities affecting fuel cell performance include fuel stream contaminants such as CO, H_2S, NH_3 and hydrocarbons [10–12], air stream contaminants such as NO_x, SO_x, CO_x, and some volatile organic compounds [13–15], as well as other impurities arising from the fuel cell components and system, such as Fe^{3+}, Cu^{2+}, Al^{3+} and Cr^{3+}, or from alloy catalysts such as Co^{2+}, Ni^{2+}, Fe^{3+}, and the like [16]. When these impurities are present in the reactant streams, fuel cell degradation or even failure can be observed, arising from deteriorated reaction kinetics, decreased ionic conductivity, and decelerated mass transport associated with changes in the structure of the catalyst layer (CL) and gas diffusion layer (GDL), and/or in the hydrophilicity/hydrophobicity ratio [7].

The research literature contains several publications on metal ion contamination in PEM fuel cells [17–20], and these publications have frequently reported that metal ions can cause membrane degradation through the ion-exchange effect. In terms of the experimental approaches, most of these studies examined the effects of metal ions by soaking the membrane electrode assembly (MEA) or membrane in solutions containing a metal ion before assembling the fuel cell [17,21–24]. Only a few studies continuously supplied metal ions into the feed streams to mimic the contamination process during fuel cell operation. For example, Pozio et al. studied Nafion® degradation in a hydrogen PEM fuel cell caused by ionic Fe that leached out continuously from stainless steel end plates [20]. Mikkola et al. conducted PEM fuel cell contamination tests by continuously injecting NaOH solution into the cathode side [25], while Yasuda et al. investigated anode degradation in a direct methanol fuel cell with Fe^{3+} and Al^{3+} in the methanol feed [31].

Since Fe^{3+} and Al^{3+} are commonly encountered metal ion impurities that can come from the water in the humidifier, metal alloy components of the fuel cell system, or Fe-containing alloy catalysts, we believe it is of great importance to study the contamination effects of these two common metals on PEM fuel cell performance. In this work, the contamination effects of Fe^{3+} and Al^{3+} on fuel cell performance at different concentrations and temperatures are reported. We also report the effects of Al^{3+} on the oxygen reduction reaction (ORR) in a three-electrode cell to help understand the contamination mechanisms of Al^{3+}.

* Corresponding author. Tel.: +1 604 221 3087; fax: +1 604 221 3001.
E-mail address: jiujun.zhang@nrc-cnrc.gc.ca (J. Zhang).

0378-7753/$ – see front matter.
doi:10.1016/j.jpowsour.2010.07.003

2. Experimental

2.1. Fuel cell contamination tests

2.1.1. Contamination testing set-up and membrane electrode assemblies

The experimental set-up and MEAs used for the contamination tests have been previously described in Ref. [26]. Briefly, the set-up consisted of a Teledyne fuel cell hardware (50 cm^2 H-50), a Fideris 100 W fuel cell test station, and a liquid injection unit. The single-cell hardware had gold-coated end plates that were heated by a pair of silicon rubber heating pads attached to the outsides of the two end plates. The graphite flow-field plates were fabricated in-house using single serpentine flow channels with 1.2 mm width, 1.0 mm channel depth and 1.0 mm landing. The MEA was assembled using an Ion Power® catalyst coated membrane (CCM) made of Nafion® 211 membrane and SGL GDLs with 20% PTFE. The catalyst loading was 0.4 mg cm^{-2} Pt on both anode and cathode sides. A fresh MEA was employed for each contamination test. The liquid injection unit consisted of a high-resolution micro-pump (Smartline Model 100 HP) to continuously deliver solutions containing $Fe(ClO_4)_3$ and $Al_2(SO_4)_3$, respectively, into the air stream ($Fe(ClO_4)_3$ was used as Fe^{3+} salt rather than $Fe_2(SO_4)_3$ due to its high solubility in aqueous solution. The amount of water brought into the system through liquid injection was compensated for by lowering the dew point of the humidifier accordingly to maintain the desired relative humidity (RH) in the fuel cell. The validation tests of the injection unit were performed at 1.0 A cm^{-2} current density with and without the injection of liquid water, using calculation-adjusted dew points [26]. It was confirmed that the variation in cell performance between the regular test system (without water injection) and the contamination test system (with water injection) was less than 9 mV. The concentrations of the two metal ions were relative to the air flow rates.

2.1.2. Testing conditions

Separate contamination tests were first conducted with 5 ppm mol Fe^{3+} mol air and 5 ppm mol Al^{3+} mol air at a current density of 1.0 A cm^{-2}. Other operating conditions were: 100% fuel cell RH, 80 °C cell temperature, 15 psig backpressure and 1.5/3.0 H_2/air stoichiometries. The effect of temperature on Fe^{3+} contamination was also studied at three temperatures, 40, 60 and 80 °C, all with 5 ppm mol Fe^{3+} mol air in the air stream while the other conditions remained the same.

2.1.3. Diagnostic measurements

All contamination tests were carried out in a constant-current discharge mode controlled by a load bank. Changes in cell impedance caused by metal ion contamination was measured with a Solartron 1252 frequency response analyzer during the contamination tests. The impedance spectra were recorded by sweeping frequencies over the range of 0.1–10 kHz. Scanning electron microscopy (SEM) analysis was performed to examine physical changes in the cross-sections of the contaminated MEAs.

2.2. Electrochemical study of the ORR in the presence of Al^{3+} in a three-electrode cell

Electrochemical measurements were conducted in a standard three-electrode electrochemical cell using an RDE set-up, with a Solartron 1287 potentiostat for controlling disk current and an AFMRX rotator (Pine Instruments) for controlling the rotating speed. A glassy carbon (GC) disk electrode (geometric area 0.247 cm^2), a platinum-black coated Pt wire and a mercury sulfate electrode were used as the working, counter and reference electrodes, respectively. The cell temperature was controlled by a water bath. Prior to each experiment, the GC disk electrode, which served as the substrate for the Pt/C catalyst, was polished to a mirror finish with 0.05 μm alumina (Buehler).

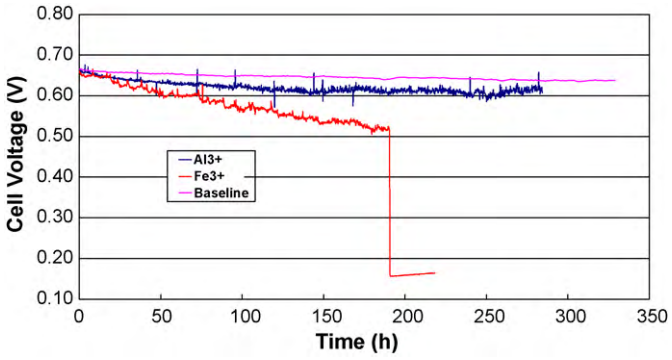

Fig. 1. Cell voltage vs. time at 1.0 A cm^{-2} with 5 ppm Al^{3+} and 5 ppm Fe^{3+}, respectively, in the air stream. Operating conditions: stoichiometries of air/H_2: 3.0/1.5; cell temperature: 80 °C; RH of the fuel cell: 100%; backpressure: 15 psig.

A commercially available Pt catalyst supported on carbon (46.9 wt.% Pt from TKK) was used to make a thin-film electrode with a Pt loading of 40 μg cm^2. We have previously reported the catalyst ink recipe and the casting of the catalyst onto the GC disk [26]. The Al^{3+}-containing electrolyte was made by dissolving $Al_2(SO_4)_3$ into 0.5 M H_2SO_4 solution. Three electrolytes were used to study the effect of Al^{3+} on the ORR: (1) 0.5 M H_2SO_4, (2) 0.5 M H_2SO_4 + 0.05 M Al^{3+} and (3) 0.5 M H_2SO_4 + 0.2 M Al^{3+}. The ORR measurements were carried out using linear sweep voltammetry between 0.05 and 1.0 V vs. RHE at 5 mV s^{-1} in an O_2-saturated electrolyte.

3. Results and discussion

3.1. Effects on fuel cell performance of 5 ppm Al^{3+} and Fe^{3+} in the air stream

Fig. 1 shows the fuel cell contamination test results at 1.0 A cm^{-2} with 5 ppm Al^{3+} and 5 ppm Fe^3 in the air stream. The presence of 5 ppm Al^{3+} or 5 ppm Fe^{3+} caused fuel cell performance to drop almost immediately after the introduction of the contaminants. However, the adverse effect of 5 ppm Fe^{3+} was much more significant than that of 5 ppm Al^{3+}, as reflected by cell performance drops of 136 mV for Fe^{3+} vs. 56 mV for Al^{3+} within 190 h. In addition, the presence of Fe^{3+} resulted in sudden death of the fuel cell. This phenomenon of fuel cell sudden death in the presence of Fe^{3+} was repeatable in all tests with Fe^{3+}. This sudden death is likely related to Fenton's reactions, which produce hydroxyl radicals and subsequently cause membrane failure. First, Fe^{3+} ions immobilized on Nafion® membrane in the presence of peroxide can produce radicals by reduction into Fe^{2+} through a modified Fenton's reaction [20,27]:

$$\text{Nafion} - Fe^{3+} + H_2O_2 \rightarrow \text{Nafion} - Fe^{2+} + HO_2^{\bullet} + H^+ \quad (1)$$

Peroxide is present as a by-product of the ORR on Pt. Secondly, the Fe^{2+} ions in Reaction (1) can also react with peroxide to produce hydroxyl radicals via Reaction (2):

$$\text{Nafion} - Fe^{2+} + H_2O_2 \rightarrow \text{Nafion} - Fe^{3+} + HO^{\bullet} + OH^- \quad (2)$$

The hydroxyl radical is considered one of the most reactive chemical species known and can in the long term degrade Nafion® polymer chains, resulting in fluoride loss and reduced conductivity [27]. Hydroxyl radicals can also damage the membrane by attacking the H-containing terminal bonds present in the polymer (i.e., H-abstraction) [5,28], which can result in the formation of membrane pinholes.

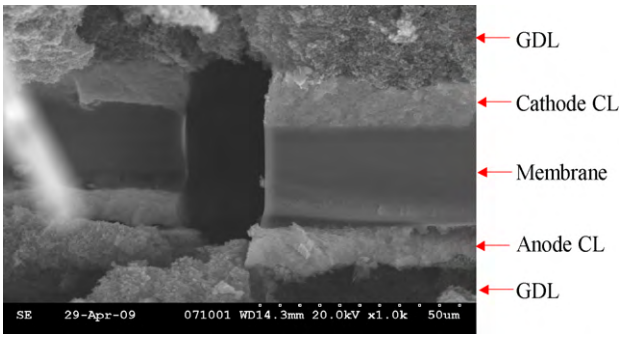

Fig. 2. SEM image of a cross-section of an MEA contaminated by 5 ppm Fe^{3+} for 190 h. Various "pinholes" with widths of about 10–15 μm are observable.

The dramatic increase in hydrogen cross-over current density from ~5.8 mA cm^{-2} before Fe^{3+} contamination to more than 50 mA cm^{-2} after contamination (exceeding the measurable limit of the potentiostat) as well as the severe leak(s) in the MEA at the end of the test provided strong evidence for the formation of membrane pinholes.

To help understand the mechanisms of Fe^{3+} contamination, SEM and EDX area scanning were conducted on several cross-sections of the MEA contaminated by 5 ppm Fe^{3+}. Fig. 2 shows one cross-section that has several "pinholes" with widths of about 10–15 μm. This further confirms the formation of pinholes caused by hydroxyl radicals, as discussed earlier. Fig. 3 shows an SEM image of another cross-section, along with elemental analysis derived from EDX area scanning at spots indicated in the SEM image. Two observations can be made from Fig. 3: (1) Fe ions, as either or both Fe^{2+} and Fe^{3+}, migrated through the membrane from the cathode side to the anode catalyst layer (ACL), (2) the membrane at the anode side became dry and twisted, which might have been caused by the formation of H_2O_2 and/or by Fe^{3+} reducing the water transport flux from the cathode to the anode side [29]. However, the low level of Fe^{3+} seen in the catalyst coated membrane (CCM) is not

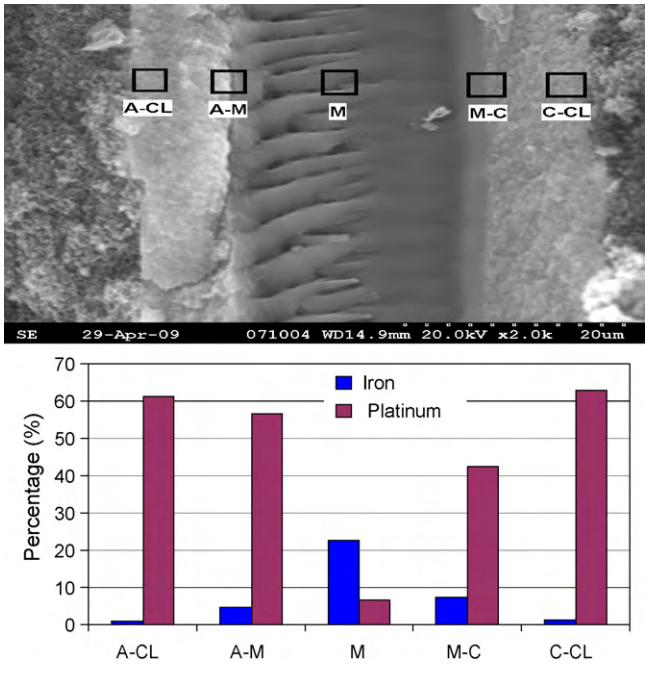

Fig. 3. Top: SEM image of a cross-section of an Fe^{3+}-contaminated MEA. Bottom: Fe and Pt distributions (atomic %) along the MEA cross-section. A–CL: anode catalyst layer; A–M: interface between anode catalyst layer and membrane; M: membrane; M–C: interface between membrane and cathode catalyst layer; C–CL: cathode catalyst layer.

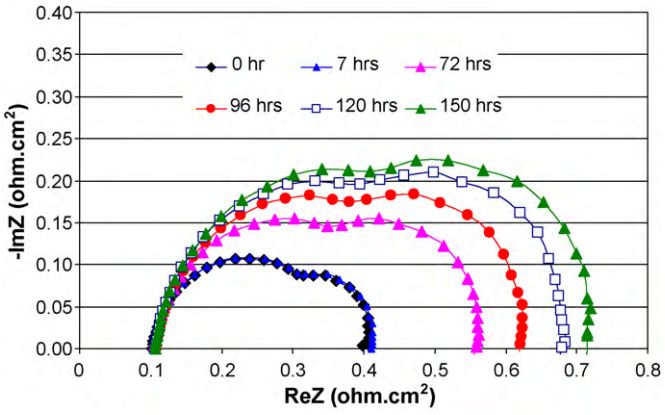

Fig. 4. Nyquist plots vs. time for the contamination test with 5 ppm Fe^{3+}. Operating conditions: current density: 1.0 A cm^{-2}; stoichiometries of air/H_2: 3.0/1.5; cell temperature: 80 °C; RH of the fuel cell: 100%; backpressure: 15 psig.

consistent with the amount injected into the cell during the contamination test, suggesting that most of the ions just by-passed the CCM on the outside of the diffusion media. To explain this observation, we proposed in our previous publication [30] that metal ions were moving against the potential gradient and the flow of protons across the membrane, and thus were not able to thoroughly replace the protons.

3.2. AC impedance measurements

Figs. 4 and 5 show the AC impedance spectrum (Nyquist plot) of the fuel cell during contamination tests in the presence of 5 ppm Fe^{3+} and 5 ppm Al^{3+}, respectively. Clearly, in both cases the charge transfer and mass transfer resistances increased significantly as a result of contamination. The increase in charge transfer resistance may relate to the effect of Fe^{3+} and Al^{3}+ on the ORR kinetics and mechanism, and the increase in mass transfer resistance may be associated with the increase in catalyst layer hydrophilicity caused by metal ion contamination. However, the increases in membrane resistance were not as significant as one would expect due to the incomplete replacement of protons by metal ions as explained earlier.

3.3. Effect of temperature on Fe^{3+} contamination

The effect of temperature on Fe^{3+} contamination was investigated at three temperatures (40, 60 and 80 °C) at 1.0 A cm^{-2} with

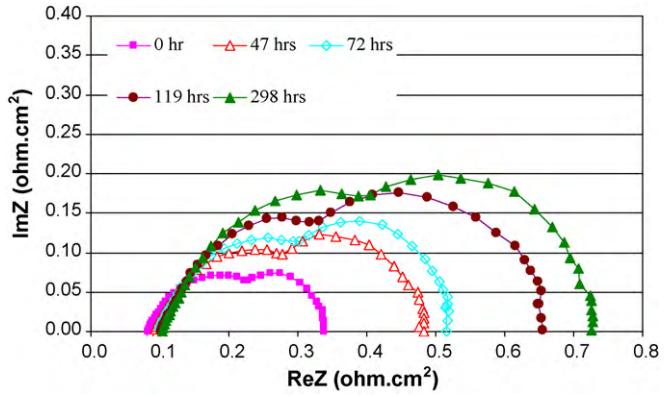

Fig. 5. Nyquist plots vs. time for the contamination test with 5 ppm Al^{3+}. Operating conditions: current density: 1.0 A cm^{-2}; stoichiometries of air/H_2: 3.0/1.5; cell temperature: 80 °C; RH of the fuel cell: 100%; backpressure: 15 psig.

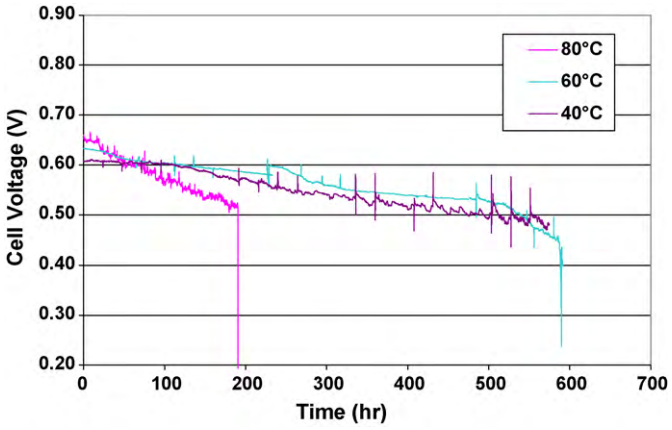

Fig. 6. Cell voltage vs. time at 40, 60 and 80 °C, respectively, with 5 ppm Fe^{3+} in the air stream. Operating conditions: current density: 1.0 A cm^{-2}; stoichiometries of air/H_2: 3.0/1.5; cell temperature: 80 °C; RH of the fuel cell: 100%; backpressure: 15 psig.

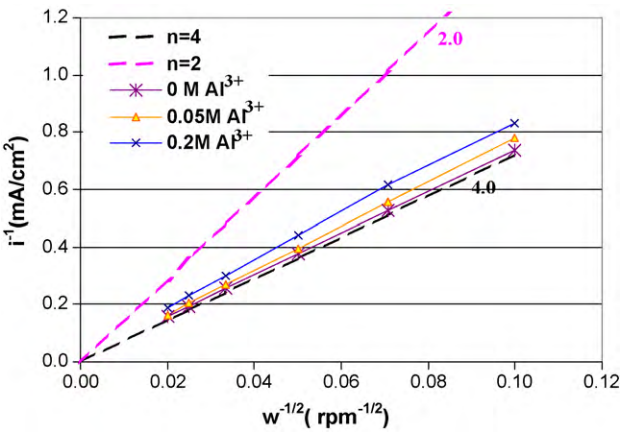

Fig. 8. Koutecky–Levich plots for the ORR on a GC RDE coated with TKK Pt/C catalyst (Pt loading: 40 μg cm^{-2}) at 25 °C in O_2-saturated 0.5 M H_2SO_4 solutions containing 0, 0.05 and 0.2 M Al^{3+}, respectively. Potential scan rate: 5 mV cm^{-2}.

5 ppm Fe^{3+}. Cell voltage vs. time plots are presented in Fig. 6. As mentioned earlier, in all three tests the fuel cell experienced early sudden death due to insufficient cell voltage, even though the membrane resistance did not seem to increase significantly, as shown in Fig. 4. In addition, the contamination effect of 5 ppm Fe^{3+} became more severe as the temperature increased. This is opposite to the effect of temperature on Co^{2+} contamination reported in our previous publication [30]. The contamination effect of Co^{2+} derives from its weak adsorption on the catalyst surface, thus as expected, the cell voltage loss in the presence of Co^{2+} became more significant as the temperature decreased. The Fe^{3+} contamination effect on fuel cell performance, however, is believed to be primarily caused by the radicals produced in the catalytic reactions of Fe^{3+} and Fe^{2+}, as discussed earlier. The increase in temperature consequently enhances the catalytic reactions described in Reactions (1) and (2), thus accelerating cell performance degradation.

3.4. Electrochemical study: the effect of Al^{3+} on the ORR

In order to understand the effects of metal ions on the ORR kinetics and mechanisms, RDE measurements were performed in a 0.5 M H_2SO_4 electrolyte containing various levels of Al^{3+}. The disk current was collected at 25 °C by linearly scanning the electrode potential from 1.0 to 0.2 V vs. RHE with a scan rate of 5 mV s^{-1}. Fig. 7 shows the disk current density as a function of electrode potential at

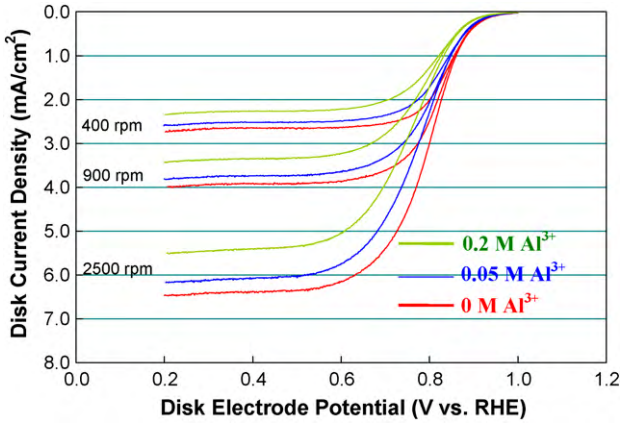

Fig. 7. Polarization curves for the ORR on a GC RDE coated with TKK Pt/C catalyst (Pt loading: 40 μg cm^{-2}) at 25 °C in O_2-saturated 0.5 M H_2SO_4 solutions containing 0, 0.05 and 0.2 M Al^{3+}, respectively. Potential scan rate: 5 mV cm^{-2}.

400, 900 and 2500 rpm rotation rates, respectively, in O_2-saturated 0.5 M H_2SO_4 electrolyte solutions containing various levels of Al^{3+}. The polarization curves obtained in the presence of Al^{3+} have lower current densities compared to the baseline (H_2SO_4 electrolyte) at all potentials, indicating that Al^{3+} led to the reduction of both kinetic and diffusion current densities for the ORR. Fig. 7 also indicates that the reduction of the ORR kinetic and diffusion limiting current densities was more evident as the concentration of Al^{3+} was increased from 0 to 0.05 and 0.2 M.

To elucidate the effects of Al^{3+} on the ORR kinetics and mechanisms, and quantitatively estimate the change in the electron transfer number of the ORR, Koutecky–Levichplots (i^{-1} vs. $\omega^{-1/2}$) were obtained to correlate the disk current densities (i) with the rotating rate (ω). Fig. 8 shows plots for the ORR with 0.05 and 0.2 M Al^{3+} present in the electrolyte solution, together with theoretical plots for the 2-electron and 4-electron transfer processes of the ORR, respectively. In the absence of Al^{3+}, the plot is almost parallel with the theoretical 4-electron process, suggesting that the ORR on Pt/C is a process very close to the 4-electron process that yields water as the major product; the electron transfer number was calculated to be 3.95. However, when 0.05 and 0.2 M Al^{2+} were added into the 0.5 M H_2SO_4 electrolyte, the slopes of the Koutecky–Levich plots increased, indicating that the presence of Al^{3+} shifted the ORR mechanisms more towards the 2-electron process that produces H_2O_2. The change on the overall electron transfer number in the presence of Al^{3+} represents the effect of Al^{3+} on the ORR mechanisms. In addition, the reduction of the electron transfer number of ORR in the presence of Al^{3+} also explains the reduction of diffusion limiting current density through Kotechy–Levich equation below:

$$\frac{I_d}{A} = i_d = 0.62nFC_{O_2}D_{O_2}{}^{2/3}\nu^{-1/6}\omega^{1/2} \quad (3)$$

where I_d is the disk plateau current (diffusion limiting current), i_d is the disk plateau current density (diffusion limiting current density), A is the electrode diffusion area, n is the overall number of transferred electrons in the ORR process, F is the Faradaic constant, C_{O_2} is the oxygen concentration, D_{O_2} is the oxygen diffusion coefficient, ν is the kinematic viscosity of the electrolyte and ω is the electrode rotation rate. It can be seen from Eq. (3) that if n is reduced in this equation, the diffusion limiting current density will definitely become smaller.

4. Conclusions

The effects that Al^{3+} and Fe^{3+} contaminants in the air stream have on PEM fuel cell performance were studied by injecting Al^{3+}-

or Fe^{3+}-containing electrolyte into the air stream between the humidifier and the fuel cell. The separate presence of 5 ppm Al^{3+} and 5 ppm Fe^{3+} caused fuel cell performance to degrade by 65 mV in 282 h and 174 mV in 191 h, respectively. AC impedance measurements revealed that increases in the kinetic and mass transfer resistances were greater contributors to cell performance than the increase in membrane resistance in both Al^{3+} and Fe^{3+} contamination tests. For Fe^{3+} contamination, the effect of temperature was also studied, and it was concluded that the severity of the adverse effect of Fe^{3+} on fuel cell performance increased with rising fuel cell temperature. In addition, the presence of Fe^{3+} caused the formation of pinholes in the membrane, which were not only evidenced by the sudden death of the fuel cell during all of the Fe^{3+} contamination tests, but also confirmed by SEM analysis. The detrimental effect of Fe^{3+} on the membrane may be ascribed to the catalytic effect of iron species in the production of hydrogen peroxide radicals that can attach to and damage the membrane.

RDE tests indicated that the presence of Al^{3+} not only changed the ORR mechanisms from a more 4-electron pathway towards a more 2-electron pathway, but also reduced the ORR kinetics.

Acknowledgments

The authors gratefully acknowledge financial support from the Institute for Fuel Cell Innovation, National Research Council of Canada (NRC–IFCI), Ballard Power Systems Inc., Hydrogenics Corp. and Angstrom Power Inc.

References

[1] W. Bi, G. Gray, T. Fuller, Eelctrochem. Solid-State Lett. 10 (5) (2007) B101.
[2] S. Zhang, X.Z. Yuan, J.N.C. Hin, H.J. Wang, K.A. Friedrich, M. Schulze, J. Power Sources 194 (2009) 588.
[3] N. Giordano, P.L. Antonucci, E. Passalacqua, L. Pino, A.S. Arico, K. Kinoshita, Electrochim. Acta 36 (1991) 1931.
[4] S.C. Ball, S.L. Hudson, D. Thompsett, B. Theobald, J. Power Sources 171 (2007) 18.
[5] A. Collier, H.J. Wang, X.Z. Yuan, J.J. Zhang, D.P. Wilkinson, Int. J. Hydrogen Energy 31 (2006) 1838.
[6] E. Endoh, S. Terazono, H. Widjaja, Y. Takimoto, Electrochem. Solid-State Lett. 7 (2004) A209.
[7] X. Cheng, Z. Shi, N. Glass, L. Zhang, J.J. Zhang, D. Song, Z.S. Liu, H.J. Wang, J. Power Sources 165 (2007) 739.
[8] N. Rajalakshmi, T.T. Jayanth, K.S. Dhathathreyan, Fuel Cells 3 (2003) 177.
[9] T. Rockward, I.G. Urdampilleta, F.A. Uribe, E.L. Brosha, B.S. Pivovar, F.H. Garzon, ECS Trans. 11 (1) (2007) 821.
[10] Y. Si, R. Jiang, J.C. Lin, H.R. Kunz, J.M. Fenton, J. Electrochem. Soc. 151 (11) (2004) A1820.
[11] R. Mohtadi, W.K. Lee, J.W.V. Zee, Appl. Catal. B: Environ. 56 (2005) 37.
[12] F.A. Uribe, S. Gottesfeld, T.A. Zawodzinski, J. Electrochem. Soc. 149 (3) (2002) A292.
[13] N. Ramasubramanian, J. Electroanal. Chem. 64 (1975) 21.
[14] H. Li, J.L. Zhang, Z. Shi, D. Song, K. Fatih, S. Wu, H. Wang, J.J. Zhang, N. Jia, S. Wessel, R. Abouatallah, N. Joos, J. Electrochem. Soc. 156 (2009) B252.
[15] H. Li, J.L. Zhang, K. Fatih, Z. Wang, Y. Tang, Z. Shi, S. Wu, D. Song, J.J. Zhang, N. Jia, S. Wessel, R. Abouatallah, N. Joos, J. Power Sources 185 (2008) 272.
[16] H. Li, Z. Shi, J.J. Zhang, in: J. Garch (Ed.), Encyclopedia of Electrochemical Power Sources, Elsevier, Oxford, UK, 2010, Ch. 874.
[17] T. Okada, N. Nakamura, J. Electrochem. Soc. 144 (1997) 2744.
[18] T. Okada, J. Electroanal. Chem. 465 (1999) 1.
[19] M. Kelly, B. Egger, G. Fafilek, J.O. Besenhard, H. Kronberger, G.E. Nauer, Solid State Ionics 176 (2005) 2111.
[20] Pozio, R.F. Silva, M.D. Francesco, L. Giorgi, Electrochim. Acta 48 (2003) 1543.
[21] T. Okada, S.M. Holst, o. Gorseth, S. Kjelstrup, J. Electroanal. Chem. 442 (1998) 137.
[22] H.L. Yeager, A. Steck, J. Electrochem. Sci. Technol. 128 (9) (1981) 1880.
[23] Kelly, B. Egger, G. Fafilek, J.O. Besenhard, H. Kronberger, G.E. Nauer, Solid State Ionics 176 (2005) 2111.
[24] T. Okada, Y. Ayato, M. Yuasa, I. Sekine, J. Phys. Chem. B 103 (1999) 3315.
[25] M.S. Mikkola, T. Rockward, F.A. Uribe, B.S. Pivovar, Fuel Cells 7 (2) (2007) 153.
[26] H. Li, K. Tsay, H.J. Wang, S. Wu, J.J. Zhang, N. Jia, S. Wessel, R. Abouatallah, N. Joos, Electrochim. Acta 55 (2010) 2622.
[27] P. Maletzky, R. Bauer, J. Lahnsteiner, B. Pouresmael, Chemosphere 38 (10) (1999) 2315.
[28] L.A. Linden, J.F. Rabek, H. Kaczmarek, A. Kaminska, M. Scoponi, Coord. Chem. Rev. 125 (1993) 195.
[29] T. Okada, in: W. Vielstich, H.A. Gasteiger, A. Lamm (Eds.), Handbook of Fuel Cells—Fundamentals, Technology and Applications, vol. 3, John Wiley & Sons, Ltd., Chichester, UK, 2003, Ch. 468.
[30] H. Li, J. Gazzarri, K. Tsay, S. Wu, H.J. Wang, J.J. Zhang, S. Wessel, R. Abouatallah, N. Joos, J. Schrooten, Electrochim. Acta 55 (2010) 5823.
[31] K. Yasuda, Y. Nakano, Y. Goto, ECS Transact. 5 (1) (2007) 291.